BioOne DIGITAL LIBRARY

Estimation and Analysis of Snow Water Equivalents Based on C-Band SAR Data and Field Measurements

Authors: Sun, Shaobo, Che, Tao, Wang, Jian, Li, Hongyi, Hao, Xiaohua, et al.

Source: Arctic, Antarctic, and Alpine Research, 47(2) : 313-326

Published By: Institute of Arctic and Alpine Research (INSTAAR), University of Colorado

URL: https://doi.org/10.1657/AAAR00C-13-135

The BioOne Digital Library (https://bioone.org/) provides worldwide distribution for more than 580 journals and eBooks from BioOne's community of over 150 nonprofit societies, research institutions, and university presses in the biological, ecological, and environmental sciences. The BioOne Digital Library encompasses the flagship aggregation BioOne Complete (https://bioone.org/subscribe), the BioOne Complete Archive (https://bioone.org/archive), and the BioOne eBooks program offerings ESA eBook Collection (https://bioone.org/esa-ebooks) and CSIRO Publishing BioSelect Collection (https://bioone.org/csiro-ebooks).

Your use of this PDF, the BioOne Digital Library, and all posted and associated content indicates your acceptance of BioOne's Terms of Use, available at www.bioone.org/terms-of-use.

Usage of BioOne Digital Library content is strictly limited to personal, educational, and non-commmercial use. Commercial inquiries or rights and permissions requests should be directed to the individual publisher as copyright holder.

BioOne is an innovative nonprofit that sees sustainable scholarly publishing as an inherently collaborative enterprise connecting authors, nonprofit publishers, academic institutions, research libraries, and research funders in the common goal of maximizing access to critical research.

Downloaded From: https://complete.bioone.org/journals/Arctic,-Antarctic,-and-Alpine-Research on 16 Mar 2025
Terms of Use: https://complete.bioone.org/terms-of-use

Arctic, Antarctic, and Alpine Research, Vol. 47, No. 2, 2015, pp. 313–326

Estimation and analysis of snow water equivalents based on C-band SAR data and field measurements

Shaobo Sun[1,3,4]
Tao Che[1,2,5]
Jian Wang[1]
Hongyi Li[1]
Xiaohua Hao[1]
Zengyan Wang[1,3] *and*
Jie Wang[1,3]

[1]Key Laboratory of Remote Sensing of Gansu Province, Heihe Remote Sensing Experimental Research Station, Cold and Arid Regions Environmental and Engineering Research Institute, Chinese Academy of Sciences, No. 320 Donggang West Road, Lanzhou, 730000, P.R. China
[2]CAS Center for Excellence in Tibetan Plateau Earth Sciences, Chinese Academy of Sciences, No. 16 Lincui Road, Chaoyang District, Beijing 100101, P.R. China
[3]University of Chinese Academy of Sciences, No. 19A Yuquan Road, Beijing 100049, P.R. China
[4]Institute of Geographic Sciences and Natural Resources Research, Chinese Academy of Sciences, No. 11A, Datun Road, Chaoyang District, Beijing, 100101, P.R. China
[5]Corresponding author: chetao@lab.ac.cn

Abstract

The spatial distribution of the snow water equivalent (SWE) of ground snow cover is one of the most important variables for understanding and simulating cold-region hydrological processes in high mountain areas. In this paper, the characteristics of C-band synthetic aperture radar (SAR) data in an area of shallow dry snow cover were analyzed based on microwave backscattering models and field snow cover measurements. The analysis revealed that the backscattering of shallow dry snow cover was dominated by the scattering of the snow-ground interface, and the dielectric constant and roughness parameters of the underlying frozen soil were the primary factors that affected the total scattering. The dielectric constant of the soil depended on the amount of liquid water present in the soil, and the amount of liquid water was primarily determined by the soil temperature. Furthermore, the insulation properties (thermal resistance) of the snow cover affected the underlying soil temperature. Consequently, the snow cover characteristics affected the backscattering signal recorded by the SAR sensors. Based on an investigation involving ENVISAT-ASAR data and simultaneous ground-based snow observations conducted on 14 March 2008, we found that the snow temperature decreased with increasing snow depth when the snow depth was less than 20 cm, and the temperature increased with decreasing snow depth when the snow depth exceeded 20 cm. Additionally, the amount of liquid water in the underlying frozen soil rapidly increased with increasing temperature. To estimate the SWE, we used a small number of field measurements data and SAR ratio images to develop two equations. The first equation defined the relationship between the snow's thermal resistance and backscattering ratio, and the second equation yielded the SWE from the estimated thermal resistance of the snow-covered area. The root mean square and relative errors of the estimated SWE were approximately 7.41 mm and 6.17%, respectively. The derived SWE also indicated that blowing snow and sun radiation were two primary factors that determined the spatial distribution of snow cover in mountainous areas.

DOI: http://dx.doi.org/10.1657/AAAR00C-13-135

Introduction

Snow cover parameters are important in hydrological studies and water resource management. Accurate inventories of spatial and temporal variability of the snow water equivalent (SWE) and improved parameterizations and modeling of water and energy exchange processes are important for advancing the understanding of climate change and its impact on the environment (Rott et al., 2008). As increasingly sophisticated snow models are applied to water, weather, and climate research, the need for accurate snow parameters (such as the SWE, snow cover area, and snow depth) is rapidly increasing (Key et al., 2007). In mountainous areas, deriving the snow parameters from ground measurements and airborne remote sensing observations is costly and limited in scope (Che et al., 2012). Satellite remote sensing technology provides a new technique for snow monitoring. Previous studies have shown that optical remote sensing can only be used to observe snow surface properties and that the SWE cannot be derived from optical remote sensing data. Although passive microwave remote sensing has been successfully used to retrieve the SWE (Chang et al., 1987; Foster et al., 2005; Che et al., 2008; Dai et al., 2012), it is not suitable for deriving the SWE on a watershed scale because of the low spatial resolution. Compared to optical and passive microwave remote sensing, active remote sensing in the microwave band is sensitive to the majority of snow parameters (Shi and Dozier, 2000), and its resolution is moderate.

Beginning in the 1990s, scientists have extensively studied the derivation of the SWE from synthetic aperture radar (SAR) data. Ulaby and Stiles (1980) found a positive relationship between the backscattering coefficient of dry snow and the SWE at a frequency of 9 GHz. Kendra et al. (1998) found the same relationship in the C-band and X-band. Arslan et al. (2006, 1999) developed a semi-empirical backscattering model of the SWE in forested areas. Bernier and Fortin (1998) found that there was a positive relationship between the SAR backscattering coefficient and the SWE only when the soil under the snow is frozen, and this relationship did not hold for non-frozen soil conditions. During early stages of snow accumulation, the freeze-thaw cycle in the underlying snow may cause a negative correlation between the backscattering and the SWE (Arslan et al., 2011). The thermal resistance of snow affects the soil temperature, and the dielectric constant decreases with decreasing temperature when the soil temperature is below freezing. The temperature drop will be greater at a site with a lower thermal resistance and will cause the signal ratio to be smaller than at other sites (Bernier and Fortin, 1998). Accordingly, Bernier and Fortin (1998), Bernier et al. (1999), and Gauthier et al. (2001) developed methods for esti-

© 2015 Regents of the University of Colorado
1523-0430/18 $7.00

Downloaded From: https://complete.bioone.org/journals/Arctic,-Antarctic,-and-Alpine-Research on 16 Mar 2025
Terms of Use: https://complete.bioone.org/terms-of-use

mating the SWE using SAR data and a small number of field snow measurements. The relationships between backscattering and snow parameters are complex, and the microwave scattering models are the basis for understanding these complex relationships. Many surface scattering models have been developed since the 1980s, including Kirchhoff models, which consist of a geometrical optics model (GOM) and a physical optical model (POM) (Ulaby et al., 1982); the small perturbation model (SPM) (Ulaby et al., 1982); the integral equation model (IEM) (Fung, 1994; Fung and Chen, 2010); and the advanced integral equation model (AIEM) (Chen et al., 2000, 2003). The commonly used volume scattering models include the Rayleigh approximation model (Ulaby et al., 1982; Drinkwater, 1989), Mie scattering theory (Tsang et al., 2004), strong fluctuation theory (SFT) (Tsang and Kong, 1981; Jin and Kong, 1984), and the dense-medium radiative transfer (DMRT) model (Tsang et al., 1985). In this study, we used the IEM and Rayleigh approximation models to analyze the surface scattering, volume scattering, and total scattering characteristics of dry snow. Based on the models and field measurements analyses, we attempted to estimate the SWE in our study area using SAR data and a small number of field measurements. Finally, the estimated SWE mapping was validated using field (in situ) snow measurement data.

The paper is organized into six sections. The study area, SAR data, and field snow measurements are described in the first section. In the second section, the backscattering coefficients simulated using the microwave radiative transfer models are presented and analyzed. Details of the SWE retrieval methodology are presented in the third section, and the estimated SWE values are validated in the fourth section. The fifth section presents a discussion of the findings. The conclusions and directions for future study are provided in the last section.

STUDY AREA AND DATA

As a component of the Watershed Allied Telemetry Experimental Research (WATER) project (Li et al., 2009a), we performed the Cold Regions Hydrological Remote Sensing and Ground-based Synchronous Observation Experiment near the upper reaches of the Heihe River in March 2008 (Wang et al., 2009). We selected the Binggou watershed as the study area for the snow remote sensing study, and basic snow parameters were measured simultaneously during the EVISAT-ASAR transit on 14 March 2008.

STUDY AREA

The Binggou watershed has an area of 30.48 km^2 and is located on the edge of the Qinghai-Tibet plateau (Fig. 1). The watershed is in the upstream portion of the Heihe River basin at elevations between 3428 m and 4400 m. The majority of the terrain

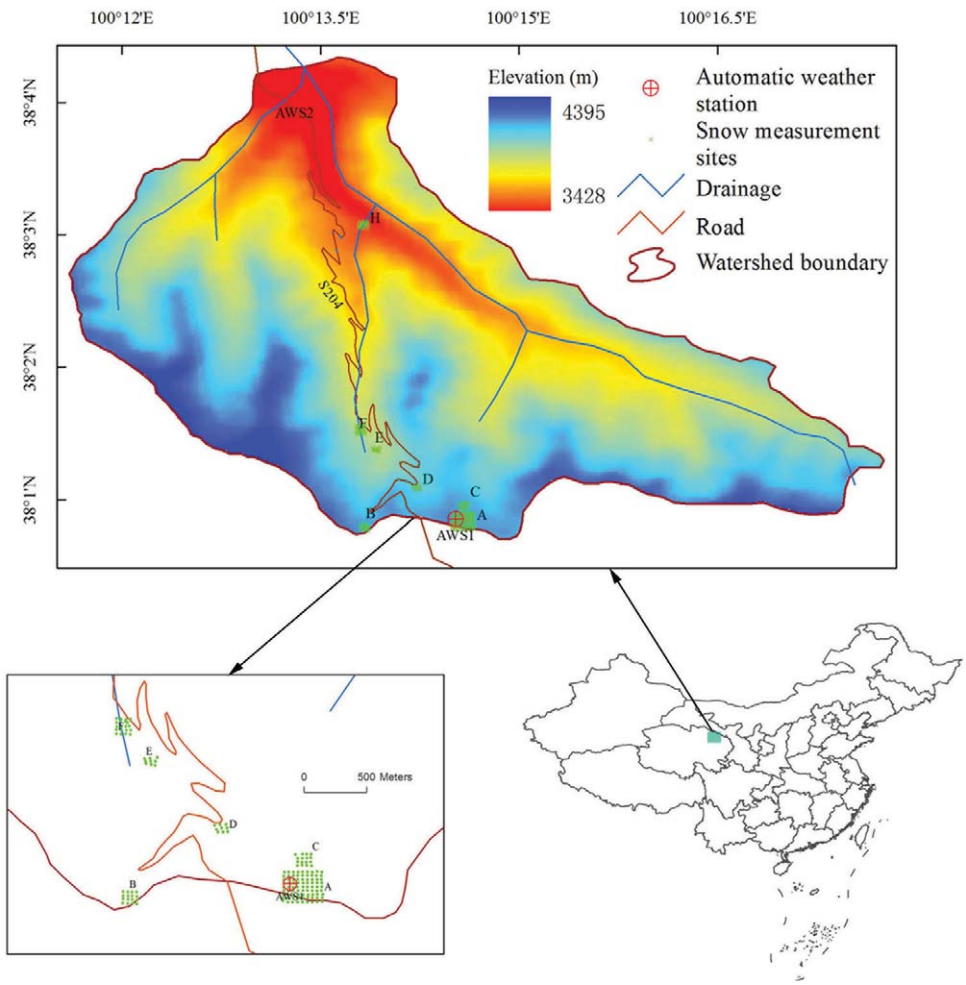

FIGURE 1. Location of the study area and field measurement sites.

Downloaded From: https://complete.bioone.org/journals/Arctic,-Antarctic,-and-Alpine-Research on 16 Mar 2025
Terms of Use: https://complete.bioone.org/terms-of-use

TABLE 1

ENVISAT-ASAR data sets used in the SAR snow cover study.

Date[a]	Time (UTC)	(A/D)[b]	Beam	Center incidence angle(°)	Snow condition
2008.03.14	15:22	A	IS7	43	Dry snow
2009.09.06	03:08	A	IS6	40	Snow free

[a]Dates are in the form yyyy.mm.dd.
[b]A, ascending. D, Descending.

below elevation 3950 m is characterized by alpine meadows, and the terrain above elevation 3950 m primarily consists of bare rocks and weathered gravel. The majority of the soil is seasonally frozen; however, at an elevation of 3500 m, the soil below a depth of 50 cm remains frozen until late May. More snow falls during the spring and autumn than during the winter (Li et al., 2009a; Wang et al., 2009; Li et al., 2009b).

SAR DATA

The advanced synthetic aperture radar (ASAR) is the SAR sensor mounted on the European Space Agency (ESA) ENVISAT-1 satellite. This sensor operates in the C-band and provides multimode, multipolarization, high-resolution SAR data. We acquired several alternating polarization ASAR data sets of the Binggou watershed in 2008 and 2009. In mountainous areas, SAR data are affected by the topography and imaging modes, which produce layovers, shadows, and inappropriate local incidence angles. Therefore, an appropriate SAR beam mode is crucial for creating high-quality images of mountainous areas. In studies of mountainous areas, SAR data collected using a higher incidence angle were preferred (Nagler and Rott, 2004). To reduce the effect of the incidence angle on the ratio image calculation, reference data with beam modes that are the same as or similar to those of the snow data are preferred. After considering all of these issues, we selected the ASAR images of 14 March 2008 and 6 September 2009 as the snow image and reference image, respectively. Table 1 lists the details of the ASAR images.

All of the ASAR images were processed using ESA's NEST software. First, the ASAR images were calibrated to convert the SAR data to backscattering coefficient images. Then, the snow image was matched to the reference image to an accuracy of one pixel. To reduce the speckle noise of the SAR images, a Frost filter

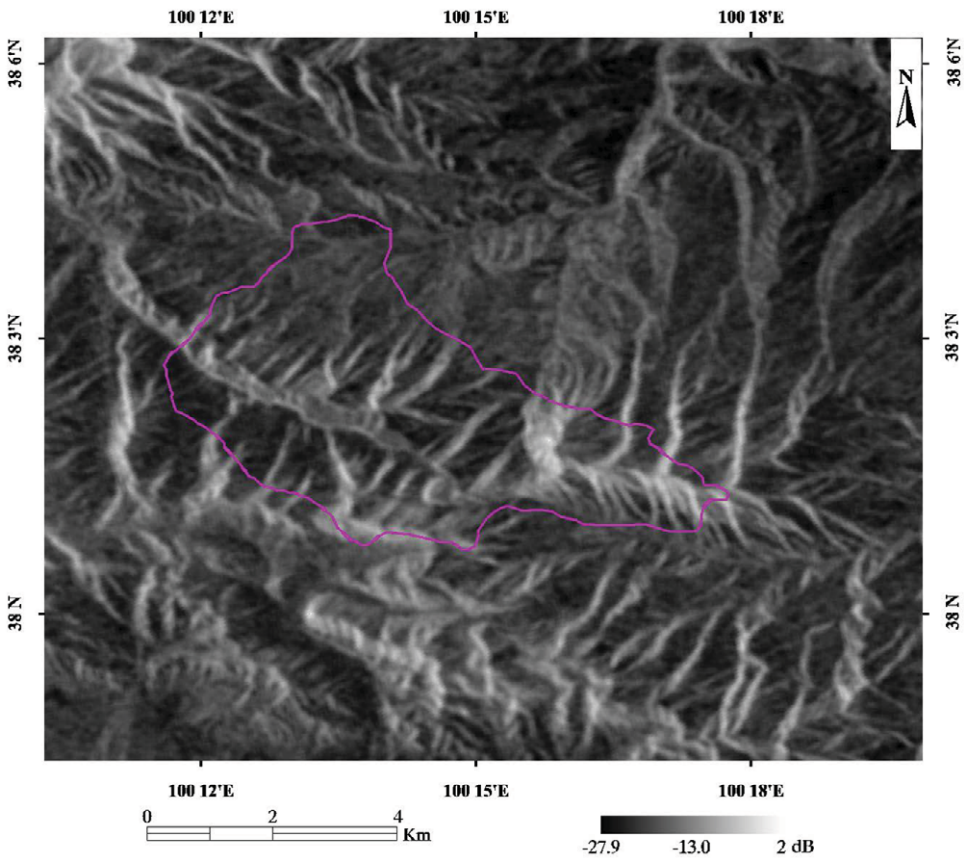

FIGURE 2. The processed EVISAT-ASAR image on 14 March 2008 (polarization, VV).

Downloaded From: https://complete.bioone.org/journals/Arctic,-Antarctic,-and-Alpine-Research on 16 Mar 2025
Terms of Use: https://complete.bioone.org/terms-of-use

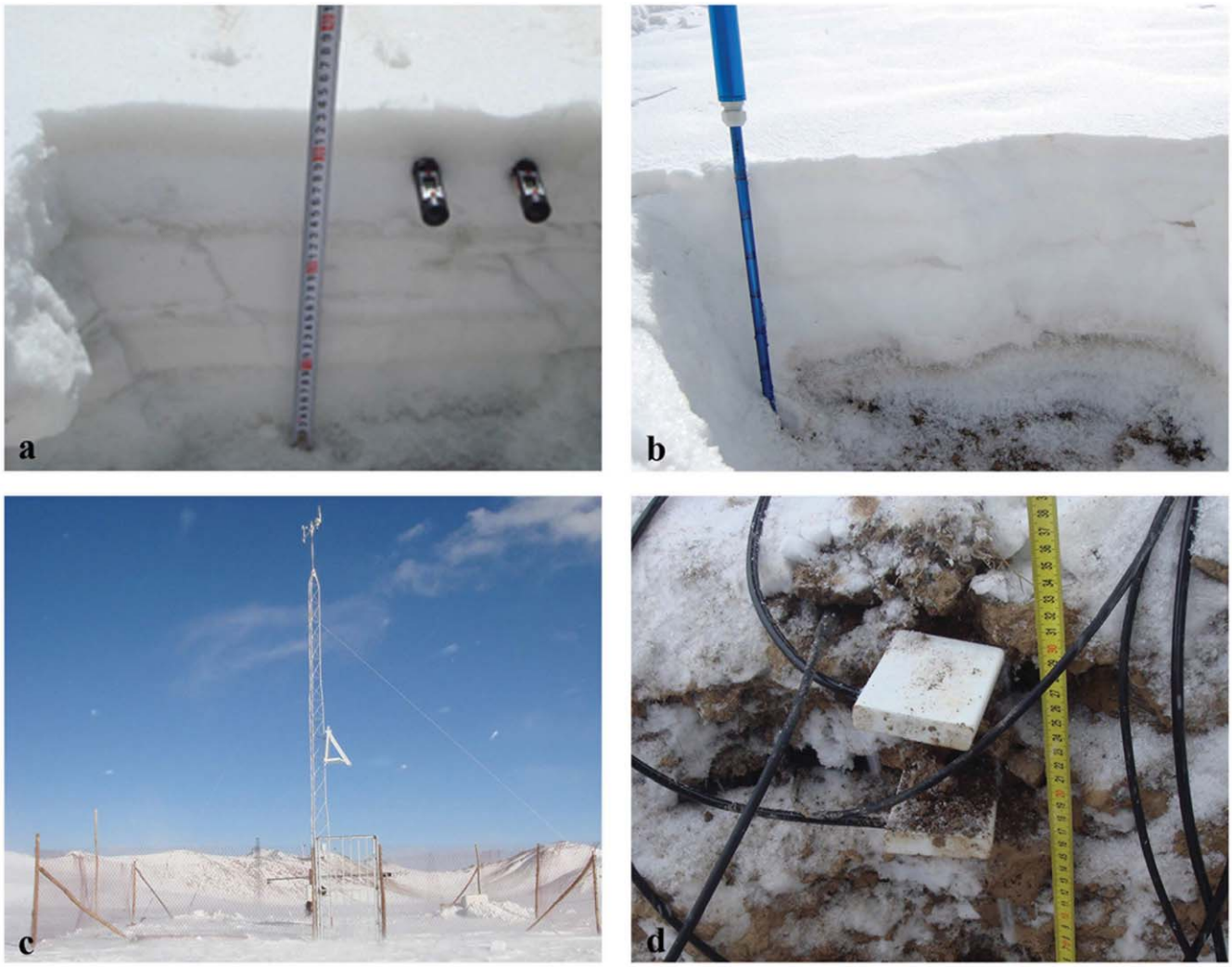

FIGURE 3. Observations of snow cover and soil parameters in the Binggou watershed. (a) Snow depth and temperature observation; (b) snow fork observation; (c) automatic weather station; and (d) soil temperature and moisture sensors.

with a 9 × 9 pixels window was applied to the images. In addition, because of the strong influence of the topography, a correction was performed using a 30 m resolution DEM (produced by ASTER GDEM) (Fig. 2). In order to get the layover-shadow pixels, a simulation process was also applied. Finally, the ratio image was calculated, and the pixels involving layover, shadowing, and inappropriate incidence angles were masked.

FIELD SNOW MEASUREMENTS

For this study, we selected seven snow cover measurement sites (Fig. 1) in the Binggou watershed and measured the snow parameters during the EVISAT-ASAR transit. Because we did not measure the parameters at site C on 14 March 2008, we will discuss only the measurement data from the other six sites in this paper. The measured parameters included the snow dielectric constant and snow density measured using snow fork, the snow temperature measured using a thermometer, the snow depth measured using a ruler (Fig. 3, parts a and b), and the snow grain size measured using an optical microscope with 80× which can read in a resolution of 0.05 mm. To obtain the meteorological data, soil parameters, and other auxiliary data, we also built two automatic weather stations in the watershed (Fig. 3, parts c and d).

Because of the high elevations, wind conditions strongly affected the snow distribution in the Binggou watershed, and the snow distribution varied substantially. At the six sites, the various parameters of the snow cover were measured at several neighboring locations. The average values and standard deviations were calculated and recorded (Tables 2 and 3). As shown in Table 2, the average snow depths at sites B and D exceeded 30 cm, and the snow depths at the other sites were 20–30 cm. The average liquid water content of the snow was less than 1% on a volume basis, the snow densities were approximately 200 kg m^{-3}, the snow grain sizes were between 0.9 and 1.2 mm, and the real parts of the snow dielectric constant were less than 1.5. The weather stations data indicated that the average wind speed in the Binggou watershed on 14 March 2008, was 3 m s^{-1} and that the air temperature was above 0 °C from 12:00 to 18:00 and below 0 °C at other times. The soil temperature was below 0 °C throughout the 24-hour measurement period. The volumetric soil moisture varied with depth, and the average volumetric water content at a depth of 5 cm was approximately 4.8%.

Downloaded From: https://complete.bioone.org/journals/Arctic,-Antarctic,-and-Alpine-Research on 16 Mar 2025
Terms of Use: https://complete.bioone.org/terms-of-use

TABLE 2

Average snow cover data measured at the field sites.

Site	Sample number	SD (cm)	SWE (mm)	Grain size (mm)	ε'[a]	ε"[b]	Density (kg m^{-3})	f_{water}[c] (%)
A	40	21	40.98	0.91	1.4054	0.0074	195.14	0.8465
B	14	34	68.73	1.03	1.4228	0.0069	202.14	0.8337
D	9	53	97.38	1.18	1.3697	0.0093	183.74	0.9446
E	9	28	47.99	1.03	1.3043	0.0052	171.39	0.5887
F	20	25	45.98	1.04	1.3668	0.0094	183.90	0.7801
H	18	20	36.40	1.07	1.3925	0.0098	182.12	0.8673

[a] ε', Real part of dielectric constant.
[b] ε", Imaginary part of dielectric constant.
[c] f_{water}, Liquid water volume fraction.

Simulation of Microwave Radiative Transfer

Electromagnetic waves of a given frequency will vary significantly, in terms of their backscatter, upon striking wet snow or dry snow. During our investigation of the Binggou watershed, the snow was dry. Therefore, only the C-band SAR backscattering of the dry snow will be discussed. For an area of snow cover with low vegetation ($h < 30$ cm), the effect of vegetation on SAR backscattering is not significant and can be ignored (Pivot, 2012). The vegetation of the Binggou watershed was primarily alpine grassland, and thus we ignored the influence of vegetation in this study.

MODEL DESCRIPTION

In general, the total backscattering signal from dry snow consists of scattering by the snow volume itself, by the snow-air interface, and by the snow-ground interface (Ulaby et al., 1986). The snow volume scattering primarily depends on the amount of energy that is transmitted into the snow and its effective penetration depth. The volume scattering of dry snow takes place from the ice grains and free-water inclusions, and its intensity is governed by their sizes and the losses caused by extinction within the layers (Ulaby et al., 1986; Drinkwater, 1989). The Rayleigh approximation model can always be used for calculating the volume scattering of dry snow (Drinkwater, 1989; Ulaby et al., 1981; Guneriussen, 1997; West, 2000) and the model is a simple and easy calculation. The model is based on the assumption that dry snow consists of small ice grains with little variation in their particle sizes, small free-water inclusions, and air, and the total volume scattering can be calculated by summing the individual backscattering components from the ice grains and water inclusions (Fung and Chen, 2010). Studies have shown the Rayleigh approximation provides accurate results for media with small spherical scatterers ($r < 0.1\lambda$) and small relative dielectric constants ($\varepsilon'' < 2$) (Ulaby et al., 1982; Fung and Chen, 2010). The model is based on the following equation:

$$\sigma_v^0 = \frac{24\pi^4 \cos\theta'}{\lambda^4 k_e}(f_1 r_1^3 |K_1|^2 + f_2 r_2^3 |K_2|^2)(1 - \frac{1}{L^2(\theta')}) \quad (1)$$

where θ' is the angle of refraction in snow; k_e is the extinction coefficient of snow and λ is the free-space wavelength; f_1 and f_2 are the volumetric fractions of ice and water scatterers, respectively; and r_1 and r_2 are the radii of the ice and water scatterers, respectively. $L(\theta')$ is the one-way propagation loss in the snowpack. K_1 is a complex quantity defined with the dielectric constant of the ice relative to the background medium, while K_2 is defined with the dielectric constant of the water relative to the background medium.

Low-frequency microwaves can easily penetrate dry snow, and the backscattering signal recorded by the SAR sensors is primarily produced by the scattering of the rough snow-ground in-

TABLE 3

The standard deviation of snow parameters at each field site.

Site	SD (cm)	SWE (mm)	Grain size (mm)	ε'	ε"	kg m^{-3}	f_{water} (%)
A	5.48	12.59	0.1726	0.0856	0.0012	27.85	0.1489
B	6.39	13.99	0.1579	0.0649	0.0011	15.29	0.1326
D	10.80	17.06	0.1593	0.0453	0.0014	6.13	0.1144
E	9.87	17.77	0.1524	0.0215	0.0009	11.13	0.0913
F	5.37	12.50	0.2508	0.0736	0.0046	15.02	0.0611
H	6.43	9.97	0.2314	0.0642	0.0038	11.20	0.0592

Downloaded From: https://complete.bioone.org/journals/Arctic,-Antarctic,-and-Alpine-Research on 16 Mar 2025
Terms of Use: https://complete.bioone.org/terms-of-use

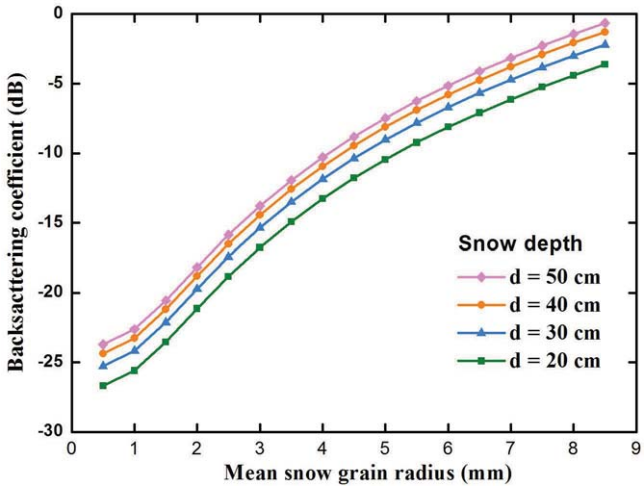

FIGURE 4. Volume scattering as a function of mean snow grain radius at various snow depths. The following parameters were used: frequencies, C band; polarization, VV; incidence angle, 45°; snow density, 187.26 kg m^{-3}; radius of water inclusions, 1.5 mm; snow dielectric constant, (1.35, –0.007); and water dielectric constant, (86, –36).

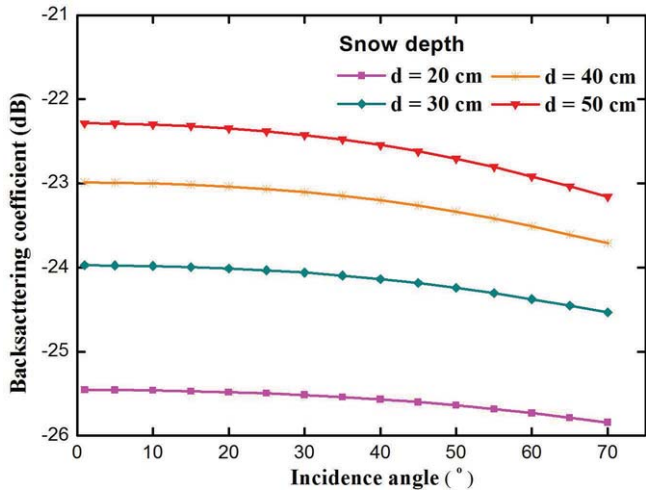

FIGURE 5. Volume scattering as a function of incidence angle and various snow depths. The following parameters were used: frequencies, C band; polarization, VV; snow density, 187.26 kg m^{-3}; radius of ice, 1 mm; radius of water inclusions, 1.5 mm; snow dielectric constant, (1.35, –0.007); and water dielectric constant, (86, –36).

terface. The IEM combines the GOM, POM, and SPM and can be applied to surfaces that vary greatly in terms of their roughness. The standard deviation of the surface height of most natural soil surfaces is small, and the single scattering term dominates. The IEM always ignores the multiple scattering terms, and its use is based on the assumption that the surface correlation function is isotropic (Gupta and Jangid, 2011). The backscattering coefficient is given by the following equation:

$$\sigma_{pp}^{0} = \frac{k^2}{4\pi}\exp(-2k^2\sigma^2\cos^2\theta)\sum_{n=1}^{\infty}|I_{pp}^{n}|^2\frac{w^n(2k\sin\theta,0)}{n!} \quad (2)$$

where p is the polarization symbol, and $p = v$ or h. The parameter $|I_{pp}^{n}|$ is given by Fung et al. (Fung et al., 1992; Fung and Chen, 2010). $w^n(2k \sin \theta, 0)$ is the Fourier transform of the nth power of the normalized surface correlation function and is given by the following equation:

$$w^n(2k\sin\theta,0) = \frac{2\pi nl^2}{[n^2+(2kl\sin\theta)^2]^{1.5}} \quad (3)$$

In the above equations, k is the wave number, ε_r is the relative dielectric constant of the medium, and θ is the incidence angle.

The IEM can be applied to a randomly rough surface over a wide range of roughness scales or frequencies and is an ideal model for a scattering surface of $k\sigma < 3$ (Fung et al., 1992). In the following section, we describe our use of the IEM in calculating the scattering caused by the snow-ground interface and snow-air interface. As studies have shown, the snow-air interface scattering is small and can always be ignored (Ulaby et al., 1986). Using the "Cloud" model (Ulaby et al., 1982), the total scattering can be determined using the following equation:

$$\sigma_{total}^{0}(\theta) = \gamma^2(\theta)[\sigma_{sv}^{0}(\theta') + \sigma_{soil}^{0}(\theta')L^{-2}(\theta')] \quad (4)$$

where $\sigma_{sv}^{0}(\theta')$ and $\sigma_{soil}^{0}(\theta')$ are the backscattering coefficients of the snow volume scattering and the snow-ground interface scattering, respectively, and $\gamma(\theta)$ is the transmission coefficient, which is calculated from the Fresnel reflection coefficient.

MODEL SIMULATION AND APPLICATION

In this section, we used the Rayleigh approximation and IEM models to analyze the surface scattering, volume scattering, and total scattering characteristics of dry snow. Figures 4 and 5 show the volume scattering calculated using the Rayleigh approximation model and the snow parameters listed in Table 2. Figure 4 shows that the volume scattering increases with increasing snow grain size and depth, and the volume scattering coefficient is less than –20 dB when the grain size is less than 1.5 mm and the snow depth is less than 50 cm. As shown in Figure 5, the volume scattering decreases with increasing incidence angle, and the effect of the incidence angle is insignificant, which may be because the C-band electromagnetic waves can easily penetrate dry snow and the refractive index of dry snow is approximately 1.

Figure 6 shows the simulation backscattering coefficient of the snow-ground interface in the Binggou watershed on 14 March 2008. For a surface of average roughness, the surface scattering decreases with an increasing incidence angle, and the scattering coefficient decreases rapidly as the incidence angle is rapidly narrowed. For any constant value of l, the scattering coefficient increases with an increasing value of σ. The scattering coeffi-

Downloaded From: https://complete.bioone.org/journals/Arctic,-Antarctic,-and-Alpine-Research on 16 Mar 2025
Terms of Use: https://complete.bioone.org/terms-of-use

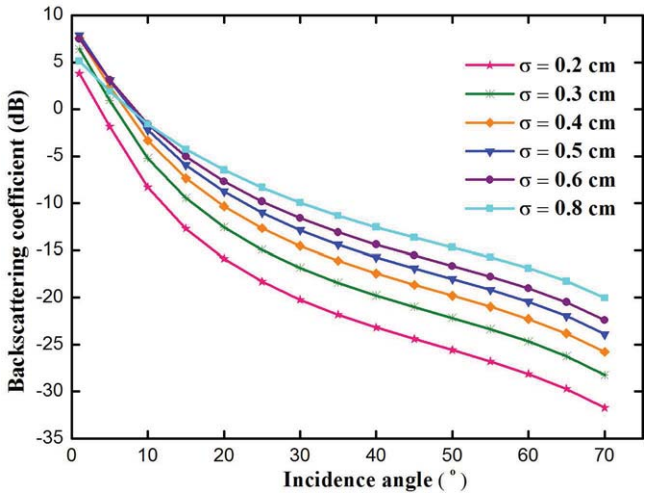

FIGURE 6. Snow/ground interface scattering as a function of incidence angle and various standard deviations of surface height. The following parameters were used: frequencies, C band; polarization, VV; correlation length, 6.5 cm; snow dielectric constant, (1.35, –0.007); and soil dielectric constant, (5.0, –0.2).

cient is greater than –20 dB when σ is greater than 0.4 and the incidence angle less than 60°. Because of the low dielectric contrast between the surface of the snow and the overlying air (West, 2000), the surface scattering of the snow-air interface is always negligible. As shown in Figure 7, the scattering due to the snow-air interface is much less than that of the snow-ground interface shown in Figure 6.

Using Equation 4, the total backscattering with various snow-ground roughness conditions was calculated and compared with the backscattering measured on 14 March 2008 (Fig. 8). The variation in the total backscattering is similar to that of the snow-ground interface backscattering, which was calculated using the IEM. Figure 8 shows that the total backscattering coefficient decreases rapidly with a decreasing incidence angle and increases with an increasing standard deviation of the height. Comparing the total backscattering coefficient with the values measured using the ASAR image, we found that the calculated and measured backscattering coefficients agree well with the σ between 0.5 and 0.6 cm. In summary, the backscattering of C-band SAR data is governed by the snow-ground interface scattering, and the dielectric constant and roughness of soil are the most important factors that determine dry snow backscattering.

Estimation of the Snow Water Equivalent

THE SWE RETRIEVAL ALGORITHM

As discussed in the previous section, the backscattering of dry snow is governed by the snow-ground interface surface scattering. The roughness of the scattering surface, the dielectric constant and other physical properties are the primary parameters that affect the backscattering. The mixture of various minerals and ice in the frozen soil has a relative dielectric constant between 2 and 4, and this value is independent of temperature (Ulaby et al., 1986). Liquid water has a high dielectric constant, and the presence of a small amount of liquid water in the soil significantly increases the soil's dielectric constant. Even at very low temperatures, a soil's dielectric constant may exceed that of ice and dry materials (Hallikainen et al., 1985; Dobson et al., 1985), which indicates that a small amount of liquid water in the soil remains unfrozen. The amount of liquid water in the frozen soil is primarily determined by the soil temperature, total water content, and soil texture. In general, the temperature is the most important factor (West, 2000). Therefore, in soil with a high liquid water content, the dielectric constant is sensitive to variations in soil temperature, particularly when the soil temperature is below 0 °C (Liou and England, 1996).

Bernier and Fortin (1998), Bernier et al. (1999), and Gauthier et al. (2001) determined that the thermal resistance

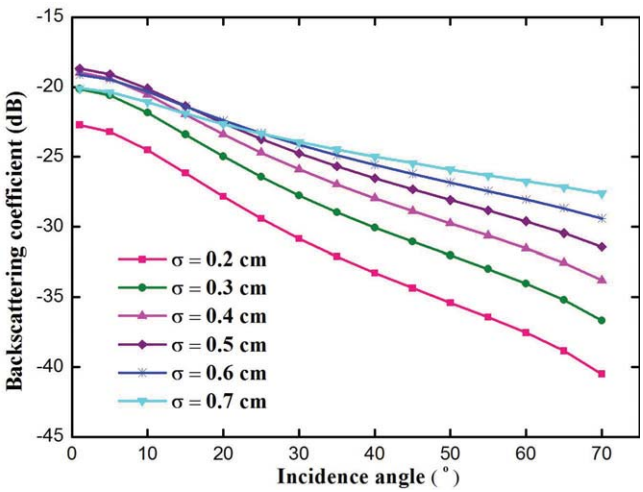

FIGURE 7. Snow/air interface scattering as a function of incidence angle and various standard deviations of surface height. The following parameters were used: frequencies, C band; polarization, VV; correlation length, 1.5 cm; snow dielectric constant, (1.35, –0.007); and air dielectric constant, (1.0, 0.0).

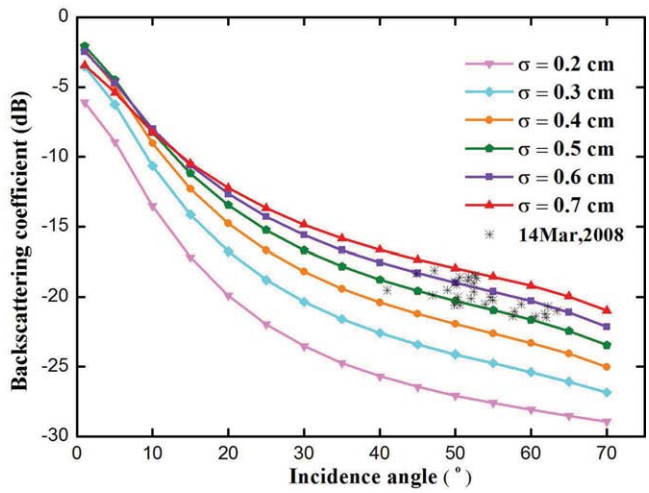

FIGURE 8. Total backscattering as a function of incidence angle and various standard deviations of surface height. The following parameters were used: frequencies, C band; polarization, VV; radius of ice, 1 mm; radius of water inclusions, 1.5 mm; correlation length of soil, 6.5 cm; snow depth, 30 cm; snow dielectric constant, (1.35, –0.007); and water dielectric constant, (86, –36).

Downloaded From: https://complete.bioone.org/journals/Arctic,-Antarctic,-and-Alpine-Research on 16 Mar 2025
Terms of Use: https://complete.bioone.org/terms-of-use

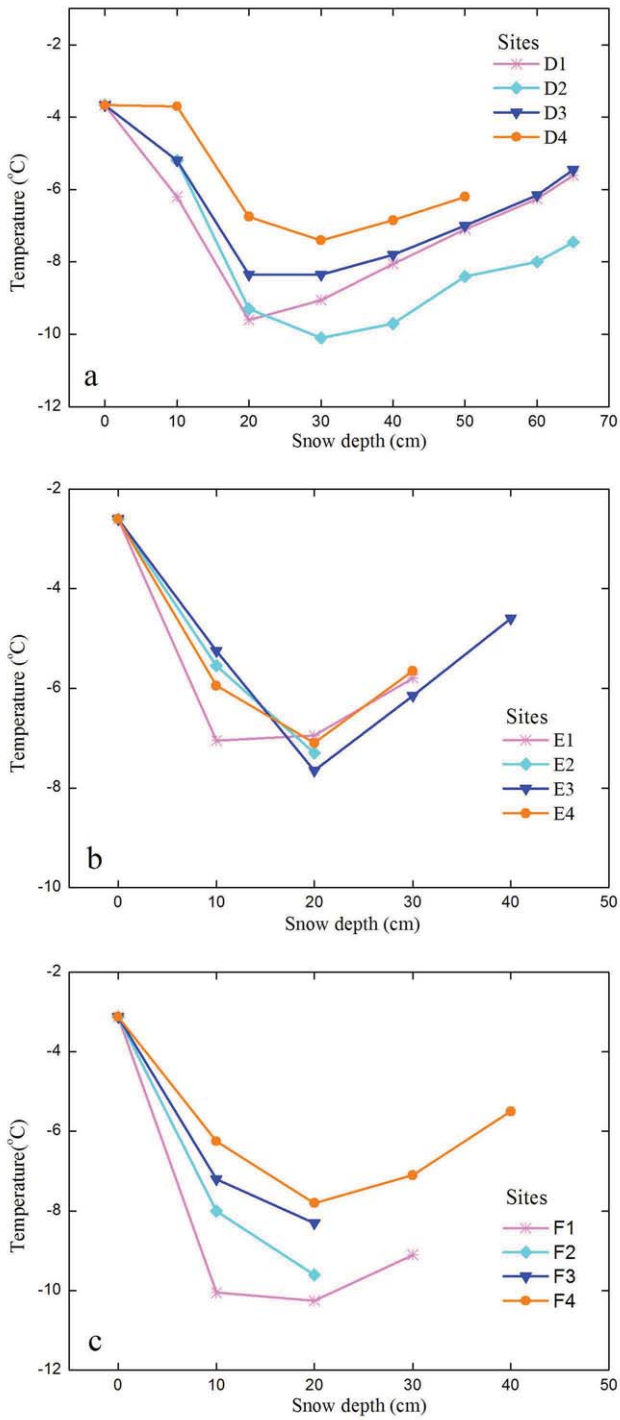

FIGURE 9. Relationships between the snow depth and temperature. (a) Site D, (b) Site E, and (c) Site F.

of snow affected the underlying soil temperature, the dielectric constant of the soil varied with the soil temperature when it was less than 0 °C, and the snow-ground interface scattering was sensitive to the soil's dielectric constant. Based on these findings, these investigators developed a method for estimating the SWE using only a few field snow measurements and SAR data. To reduce the effects of the topography and the speckle of the SAR images, a ratio image was used instead of a single snow image.

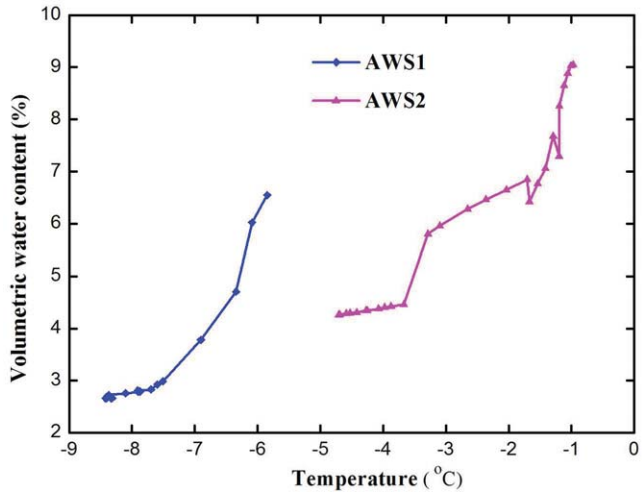

FIGURE 10. Relationship between the soil temperature and volumetric water content on 14 March 2008.

Before apply this algorithm to the Binggou watershed, we first analyzed the primary snow and soil characteristics. We used the measured snow layer data to analyze the relationship between the snow temperature and thermal resistance. As shown in Figure 9, we selected three snow pits at sites D, E, and F and analyzed the snow temperature variations at various depths. At site D, the snow temperature decreased from –3.7 °C to approximately –8 °C between the surface and a depth of 20 cm and then increased below a depth of 20 cm. The snow temperature was approximately –5 °C at a depth of approximately 65 cm. The average snow depths at sites E and F were approximately 30 cm, and the trends there were similar to those observed at site D (Fig. 9, parts b and c). This trend in varying temperatures with depth was caused by the insulation property of the snow, which was described by the following equation:

$$R = \frac{d}{C} \tag{5}$$

where R (°C m^2 s J^{-1}) is the thermal resistance, d is the snow depth, and C (J °C^{-1} m^{-1}) is the snow's thermal conductivity, which is a function of the snow's density expressed in kg m^{-3}. In this paper, C was calculated using the equation given by Raudkivi (1979):

$$C = 2.83056*10^{-6} * \rho^2 - 9.09947*10^{-5} * \rho + 0.031974 \tag{6}$$

The weather station data were used to analyze the trend in the soil's volumetric water content with variations in the soil temperature within the uppermost 5 cm (Fig. 10). As shown in Figure 10, the liquid water content increases rapidly with increasing soil temperature. The AWS1 (the weather station 1) shows that when the soil temperature increases from –9 °C to –5.8 °C, the volumetric soil water content increases from 2.6% to 6.5%. Because the elevation of AWS2 is much less than that of AWS1, the temperatures of AWS2 (the weather station 2) were higher than that of AWS1. The AWS2 shows that when the soil temperature is greater than –5 °C, the trend in the volumetric water content is in accordance with that of AWS1.

Figures 9 and 10 show that the thermal resistance of the snow cover affected the underlying soil's temperature and that the

Downloaded From: https://complete.bioone.org/journals/Arctic,-Antarctic,-and-Alpine-Research on 16 Mar 2025
Terms of Use: https://complete.bioone.org/terms-of-use

TABLE 4

Comparison of estimated average SWE values and measurement data.

Sites	Measurement SWE (mm)	Standard deviation (mm)	Estimated SWE (mm)	Standard deviation (mm)	Absolute errors (mm)
A	36.7	7.8	42.6	13.5	–5.9
B	62.5	6.7	67.0	7.7	–4.5
D	80.9	28.8	74.7	16.4	6.2
E	59.8	21.1	46.2	11.0	13.6
F	41.1	11.6	36.1	10.3	5.0
H	35.2	6.9	30.1	4.6	5.1

temperature of the underlying frozen soil determined the soil's volumetric water content. Because the soil's dielectric constant is sensitive to the soil's volumetric water content and the backscattering signal of soil is determined by the soil's dielectric constant, the snow's characteristics affect the backscattering signal recorded by the SAR sensors. Therefore, the SWE can be estimated using the snow's thermal resistance. To derive the SWE using the algorithm developed by Bernier and Fortin (1998), two equations were developed. The first equation is an exponential relationship between the snow's thermal resistance and the backscattering ratio image:

$$R = exp\,(\sigma_{ratio} + a / b) + c \qquad (7)$$

where $\sigma_{ratio} = \sigma_s - \sigma_r$; σ_s and σ_r are the backscattering coefficients of the snow image and reference image, respectively; and *a, b,* and *c* are empirically derived variables.

The second equation is a linear relationship between the snow's thermal resistance and the SWE:

$$SWE = \alpha R + \beta \qquad (8)$$

Because of the variation in snow density over a large area, α may be a function of snow density. In this study, an average value of the snow density was used, and α and β were variables that are to be derived empirically. Finally, after the coefficients in Equations 7 and 8 are determined, the *R* image can be calculated from Equation 7, and a map of the SWE can be derived from the estimated *R* image using Equation 8.

RESULTS

After all of the SAR data were processed, we calculated the ratio image and the snow thermal resistance using approximately half of the experimental data from each site (the other data were used to validate the inversion results). Figure 11 shows the relationship between the

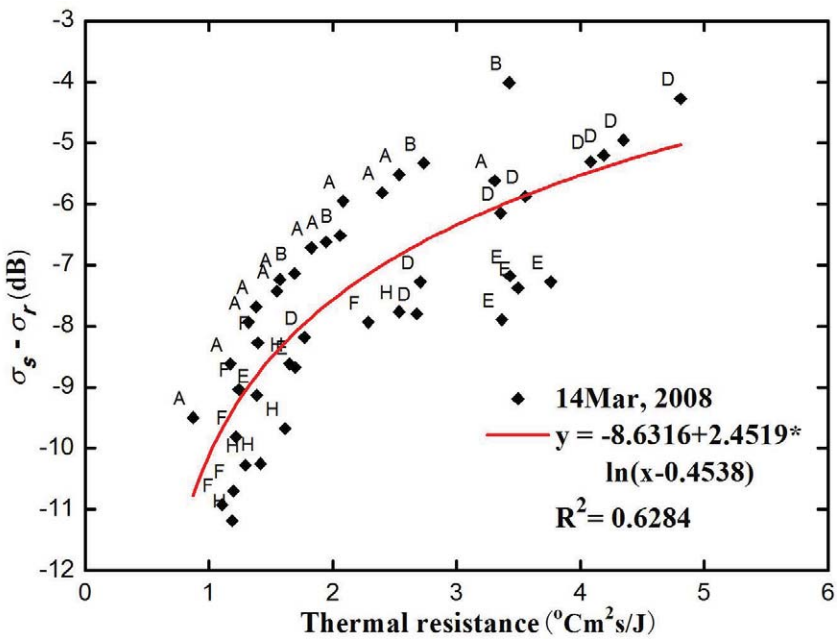

FIGURE 11. Relationship between the measured thermal resistance and the ratio image values of the field measurement sites.

Downloaded From: https://complete.bioone.org/journals/Arctic,-Antarctic,-and-Alpine-Research on 16 Mar 2025
Terms of Use: https://complete.bioone.org/terms-of-use

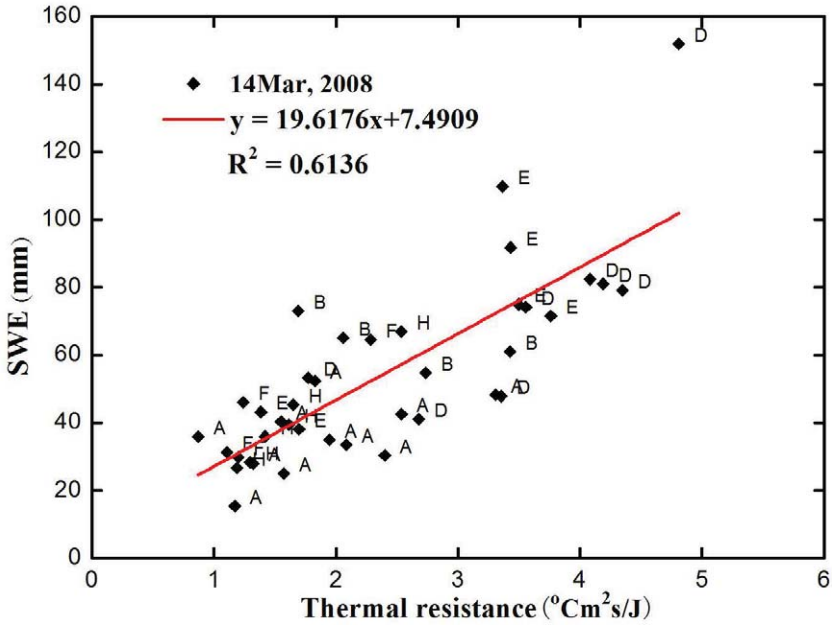

FIGURE 12. Relationship between the ratio image and the SWE measured at the field measurement sites.

ratio image values and the calculated snow thermal resistance values. All of the values of R exceed 0.5, and there is a natural logarithmic relationship between σ_{ratio} and R. Thus, Equation 7 can be written as:

$$R = \exp(\sigma_{ratio} / 2.4519 + 8.6316 / 2.4519) + 0.4538 \quad (9)$$

The snow's thermal resistance is determined by the snow depth and density. Because we assumed an average density, the values of R reflected the snow depth distribution. Sites with low thermal resistance will display large temperature drops, resulting in smaller signal ratios than those of other sites (Bernier and Fortin, 1998). The opposite is the case at sites with high thermal resistance.

By analyzing the relationship between R and SWE using a portion of the field measurement data (Fig. 12), Equation 8 can be written as

$$SWE = 19.6176R + 7.4909 \quad (10)$$

The distribution of R reflects the distribution of the snow depth. As indicated by Equation 5, the values of R increase with the snow depth; Figure 11 also shows this relationship. The snow

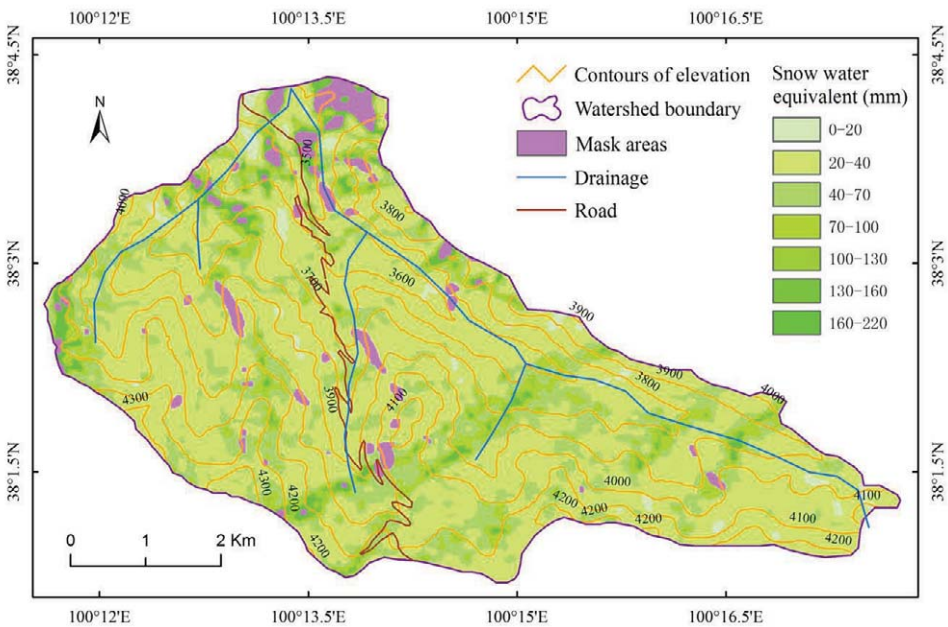

FIGURE 13. Distribution of the SWE retrieved from EVISAT-ASAR data on 14 March 2008.

Downloaded From: https://complete.bioone.org/journals/Arctic,-Antarctic,-and-Alpine-Research on 16 Mar 2025
Terms of Use: https://complete.bioone.org/terms-of-use

depths at sites D, B, and E were greater, and these sites exhibited greater thermal resistance.

When using SAR data to measure snowpack parameters in mountainous areas, topographic distortions must be considered. In this study, we excluded all pixels that were affected by layover, shadows, or inappropriate local incidence angles (Nagler and Rott, 2000; Sun et al., 2013). After all of these distorted pixels were masked, we estimated the *R* image using Equation 9 and then retrieved the SWE map using Equation 10 (Fig. 13). The SWE map shows that the SWE of the snow cover in the southern regions was generally greater than that of the northern regions and that the snow accumulations were thicker in the valley areas.

Validation

Because of the effects of the topography and wind, there was great variability in the spatial distribution of snow in the Binggou watershed (Table 2). To validate the SWE estimates, we compared the remaining SWE measurement data that were not used (described in the previous section) to the estimates of SWE (Table 4). The average estimated SWE and measured SWE values were 49.45 mm and 52.7 mm, respectively. The average mean absolute error was approximately 3 mm. The root mean square and relative errors were 7.41 mm and 6.17%, respectively. The measurement data indicated that the estimated SWE varied greatly from one site to the next. The snow cover at site H contained the minimum estimated SWE (30.1 mm), and the snow at site D contained the maximum SWE (74.7 mm). The SWE at site E exhibited the maximum mean absolute error (13.6 mm), and the SWE at site B exhibited the minimum mean absolute error (4.5 mm). The mean estimated SWE in the Binggou watershed measured 41 mm, and the maximum SWE was 215 mm. Because of the large spatial variation in the distribution of snow cover, there was a large standard deviation in the SWE data (32 mm).

Figure 13 shows that the variation in SWE measurements in the Binggou watershed is clearly due to topographic and elevation variations. The SWE of the snow cover in the higher elevation portions in the southern part of the watershed were generally greater than those of the lower elevation portions in the northern region. Due to the effects of blowing snow, snow accumulations were thicker in the valley areas, such as at site D. Solar radiation was also an important factor in the distribution of snow across the watershed. By analyzing the snow water storage and the topography, the data revealed that snow accumulated primarily on the northeast-facing slopes, followed by the north-, west-, and northwest-facing slopes. The south- and southeast-facing slopes had the least snow (Fig. 14, part a), and the snow was concentrated between elevations 3700 and 4200 m (Fig. 14, part b). These findings indicate that the distribution of snow at the lower elevations was determined by the temperature, and wind redistributed the snow in the high-elevation, vegetation-free areas.

After performing the SAR snow cover investigations on 14 March 2008, we also estimated the SWE in the Binggou watershed by way of airborne microwave radiometry on 29 March 2008 (Che et al., 2012). After comparing these microwave radiometry SWE estimates with their corresponding SAR estimates, we noted that the snow water storage estimate using SAR was slightly lower than that estimated using microwave radiometry (1.14×10^6 m^3 versus 1.18×10^6 m^3). This discrepancy was due to a snowfall event that occurred between 14 and 29 March 2008. The characteristics of the snow water storage distribution were also compared (Figs. 14 and 15). Figure 14 shows that the topographic and elevation characteristics of the radiometry SWE estimates are similar to that of the SAR SWE estimates, and there was a good agreement between the SWE estimates using the two methods.

Discussion

In this study, we used the Rayleigh approximation model and the IEM to simulate the snow volume backscattering and surface backscattering with field snow cover data. The results indicated that the volume backscattering coefficient was less than –20 dB when the snow depths were 20–50 cm and the grain sizes were 1.5 mm. The backscattering coefficient of the snow-ground interface exceeded –20 dB when the standard deviation of the height was greater than 0.4 and the incidence angle was less than 60°. Because the dielectric constant of the dry snow at the surface was similar to that of air (1.35 and 1.0, respectively) and the reflection coefficient of the snow-air interface was small, the backscattering coefficient of this interface was relatively small and was ignored. The calculated backscattering coefficient by using these models and the measured backscattering coefficient were compared. In this case, when the σ value was between 0.5 and 0.6, there was good agreement between the measured and simulated backscattering coefficients. This finding indicated that the C-band SAR backscattering coefficient of dry snow was governed by the scattering of the snow-ground interface, and the roughness parameters and dielectric constant of the soil were the factors that most strongly affected the SAR backscattering coefficient of the dry snow.

Based on the previous analysis, we estimated the SWE of the Binggou watershed using Equations 9 and 10. Although this method underestimated the SWE by approximately 3 mm, our analyses indicate that it was possible to estimate the SWE of dry shallow snow cover using C-band SAR data and a small number of ground measurements. The variations in the densities of snow layers must be taken into consideration in areas of deep snow cover, where the SWE may be a function of the snow density and thermal resistance. In addition, the parameters of Equations 9 and 10 may vary from one region to the next due to the terrain and climatic factors. The snow's depth and density determine its thermal resistance, and these variations in snow density and depth also determine the coefficients of Equations 9 and 10.

Conclusions

We performed a study of snow cover in the upper reaches of the Heihe River on 14 March 2008 using ENVISAT-ASAR data and ground-based snow observations. Specifically, we used microwave scattering models to analyze the C-band SAR scattering characteristics of snow-covered areas and estimated the distribution of the SWE using SAR data and snow cover data measured in the field. The analysis of the models indicated that the C-band SAR backscattering coefficient of the dry snow was governed by the scattering of the snow-ground interface, and the dielectric constant and roughness parameters of the soil were the primary factors that affected the dry snow backscattering. The field snow cover measurements indicated that the snow temperature decreased with

Downloaded From: https://complete.bioone.org/journals/Arctic,-Antarctic,-and-Alpine-Research on 16 Mar 2025
Terms of Use: https://complete.bioone.org/terms-of-use

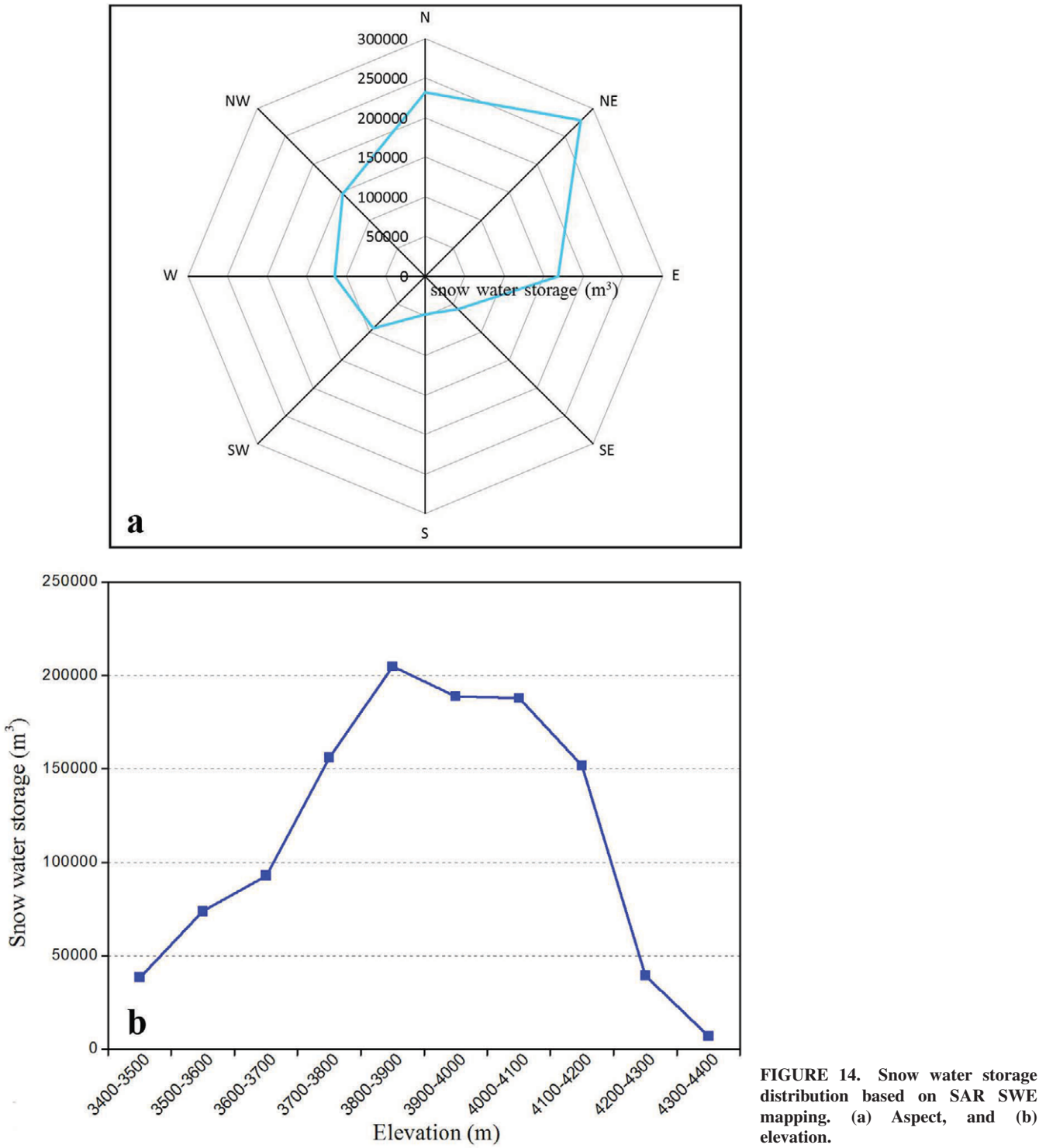

FIGURE 14. Snow water storage distribution based on SAR SWE mapping. (a) Aspect, and (b) elevation.

increasing snow depth when the snow depth was less than 20 cm, and the temperature increased with increasing snow depths below a depth of 20 cm. The soil observation data indicated that the liquid water content of the soil rapidly increased with increasing temperature. The snow thermal resistance affected the underlying soil temperature, and the amount of liquid water within the frozen soil strongly increased with the temperature. The dielectric constant of the soil was sensitive to the liquid water content, and the scattering by the snow-ground interface was strongly determined by the soil dielectric constant. In other words, the snow's thermal resistance affected the dielectric constant and the backscattering signal recorded by the SAR sensors. Accordingly, we estimated the SWE of Binggou watershed using the SAR data and limited field snow measurements, and the results indicated that the SWE was underestimated by approximately 3 mm.

This study indicates that the SWE can be estimated using C-band SAR data and a small number of snow ground measurements in areas of shallow dry snow cover, such as in northwestern China.

Downloaded From: https://complete.bioone.org/journals/Arctic,-Antarctic,-and-Alpine-Research on 16 Mar 2025
Terms of Use: https://complete.bioone.org/terms-of-use

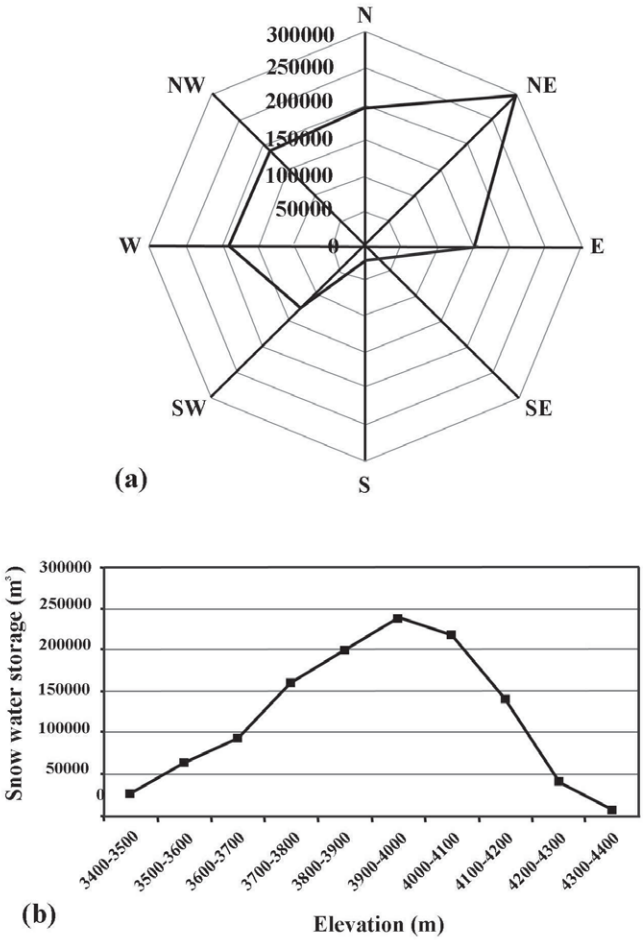

FIGURE 15. Snow water storage distribution based on radiometry SWE mapping. (a) Aspect, and (b) elevation (Che et al., 2012).

Future work may include the analysis of the backscattering characteristics of areas of deep snow cover and the retrieval of corresponding SWE maps.

Acknowledgments

The authors thank all of the participants in the 2008 WATER cold region study. This study was supported by the Chinese Academy of Sciences Project (KZCX2-XB3-15), the China State Key Basic Research Project (2013CBA01802), and the Chinese National Natural Science Foundation (41271356). The ESA provided the ASAR data in the framework of the Dragon 2 program (Project ID 5322). We thank two anonymous reviewers for their helpful comments and suggestions, which significantly improved this paper.

References Cited

Arslan, A. N., Praks, J., Koskinen, J., and Hallikainen, M. T., 1999: An empirical model for retrieving water equivalent of dry snow from C-band SAR data. *In* Proceedings, IEEE 1999 International Geoscience and Remote Sensing Symposium (IGARSS), Hamburg, Germany. Piscataway, New Jersey: Institute of Electrical and Electronics Engineers, Volume 3, 1789–1791.

Arslan, A. N., Pulliainen, J., and Hallikainen, M. T., 2006: Observations of L- and C-band backscatter and a semi-empirical backscattering model approach from a forest-snow-ground system. *Progress in Electromagnetics Research*, 56: 263–281.

Arslan, A. N., Pulliainen, J., Lemmetyinen, J., Nagler, T., Root, H., and Kern, M., 2011: Effects of snowpack parameters and layering processes at X- and Ku-band backscatter. *In* Proceedings, 2011 IEEE International Geoscience and Remote Sensing Symposium (IGARSS), Vancouver, Canada. Piscataway, New Jersey: Institute of Electrical and Electronics Engineers, 3637–3640.

Bernier, M., and Fortin, J. P., 1998: The potential of times series of C-band SAR data to monitor dry and shallow snow cover. *IEEE Transactions on Geoscience and Remote Sensing*, 36: 226–243.

Bernier, M., Fortin, J. P., Gauthier, Y., Gauthier, R., Roy, R., and Vincent, P., 1999: Determination of snow water equivalent using RADARSAT SAR data in eastern Canada. *Hydrological Processes*, 13: 3041–3051.

Chang, A. T. C., Foster, J. L., and Hall, D. K., 1987: Nimbus-7 derived global snow cover parameters. *Annals of Glaciology*, 9: 39–44.

Che, T., Li, X., Jin, R., Armstrong, R., and Zhang, T. J., 2008: Snow depth derived from passive microwave remote-sensing data in China. *Annals of Glaciology*, 49: 145–154.

Che, T., Dai, L., Wang, J., Zhao, K., and Liu, Q., 2012: Estimation of snow depth and snow water equivalent distribution using airborne microwave radiometry in the Binggou Watershed, the upper reaches of Heihe River Basin. *International Journal of Applied Earth Observation and Geoinformation*, 17: 23–32.

Chen, K. S., Wu, T. D., Tsay, M. K., and Fung, A. K., 2000: Note on the multiple scattering in an IEM model. *IEEE Transactions on Geoscience and Remote Sensing*, 38: 249–256.

Chen, K. S., Wu, T. D., Tsang, L., Li, Q., Shi, J., and Fung, A. K., 2003: Emission of rough surfaces calculated by the integral equation method with comparison to three-dimensional moment method simulations. *IEEE Transactions on Geoscience and Remote Sensing*, 41: 90–101.

Dai, L. Y., Che, T., Wang, J., and Zhang, P., 2012: Snow depth and snow water equivalent estimation from AMSR-E data based on a priori snow characteristics in Xinjiang, China. *Remote Sensing of Environment*, 127: 14–29.

Dobson, M. C., Ulaby, F. T., Hallikainen, M. T., and El-Rayes, M. A., 1985: Microwave dielectric behavior of wet soil—part II: dielectric mixing models. *IEEE Transactions on Geoscience and Remote Sensing*, 23: 35–46.

Drinkwater, M. R., 1989: LIMEX'87 ice surface characteristics: implications for C-band SAR backscatter signatures. *IEEE Transactions on Geoscience and Remote Sensing*, 27: 501–513.

Foster, J. L., Sun, C., Walker, J. P., Kelly, R., Chang, A., Dong, J., and Powell, H., 2005: Quantifying the uncertainty in passive microwave snow water equivalent observations. *Remote Sensing of Environment*, 94: 187–203.

Fung, A. K., 1994: *Microwave Scattering and Emission Models and Their Applications*. Boston: Artech House.

Fung, A. K., and Chen, K. S., 2010: *Microwave Scattering and Emission Models for Users*. Boston: Artech House.

Fung, A. K., Li, Z., and Chen, K. S., 1992: Backscattering from a randomly rough dielectric surface. *IEEE Transactions on Geoscience and Remote Sensing*, 30: 356–369.

Gauthier, Y., Bernier, M., Fortin, J. P., Gauthier, R., Roy, R., and Vincent, P., 2001: Operational determination of snow water equivalent using Radarsat data over a large hydroelectric complex in eastern Canada. *In* Proceedings, Remote Sensing and Hydrology 2000, Santa Fe, New Mexico. Intevrnational Association of Hydrological Sciences (IAHS) Publication 267: 343–348.

Guneriussen, T., 1997: Backscattering properties of a wet snow cover derived from DEM corrected ERS-1 SAR data. *International Journal of Remote Sensing*, 18: 375–392.

Gupta, V. K., and Jangid, R. A., 2011: Microwave response of rough surfaces with auto-correlation functions, RMS heights and

Downloaded From: https://complete.bioone.org/journals/Arctic,-Antarctic,-and-Alpine-Research on 16 Mar 2025
Terms of Use: https://complete.bioone.org/terms-of-use

correlation lengths using active remote sensing. *Indian Journal of Radio & Space Physics*, 40: 137–146.

Hallikainen, M. T., Ulaby, F. T., Dobson, M. C., El-Rayes, M. A., and Wu, L-K., 1985: Microwave dielectric behavior of wet soil-part II: dielectric mixing models and experimental obervations. *IEEE Transactions on Geoscience and Remote Sensing*, 23: 25–34.

Jin, Y-Q., and Kong, J. A., 1984: Strong fluctuation theory for electromagnetic wave scattering by a layer of random discrete scatterers. *Journal of Applied Physics*, 55: 1364–1369.

Kendra, J. R., Sarabandi, K., and Ulaby, F. T., 1998: Radar measurements of snow experiment and analysis. *IEEE Transactions on Geoscience and Remote Sensing*, 36: 864–879.

Key, J., Drinkwater, M., and Ukita, J., 2007: *IGOS Cryosphere Theme Report—For the Monitoring of our Environment from Space and from Earth.* WMO/TD Publication 1405: 100.

Li, H., Wang, J., Bai, Y., Li, Z., and Dou, Y., 2009b: The snow hydrological process during a representative snow cover period in Binggou Watershed in the upper reaches of Heihe River. *Journal of Glaciology and Geocryology*, 31: 293–300.

Li, X., Li, X., Li, Z., Ma, M., Wang, J., Xiao, Q., Liu, Q., Che, T., Chen, E., Yan, G., Hu, Z., Zhang, L., Chu, R., Su, P., Liu, Q., Liu, S., Wang, J., Niu, Z., Chen, Y., Jin, R., Wang, W., Ran, Y., Xin, X., and Ren, H., 2009a: Watershed Allied Telemetry Experimental Research. *Journal of Geophysical Research*, 114: D22, doi http://dx.doi.org/10.1029/2008JD011590.

Liou, Y. A., and England, A. W., 1996: Annual temperature and radiobrightness signatures for bare soils. *IEEE Transactions on Geoscience and Remote Sensing*, 34: 981–990.

Nagler, T., and Rott, H., 2000: Retrieval of wet snow by means of multitemporal SAR data. *IEEE Transactions on Geoscience and Remote Sensing*, 38: 754–765.

Nagler, T., and Rott, H., 2004: Snow classification algorithm for ENVISAT ASAR. *In* Proceedings, 2004 ENVISAT & ERS Symposium, 6–10 September, Salzburg, Austria. Noordwijk, Netherlands: European Space Agency.

Pivot, F. C., 2012: C-band SAR image for snow cover monitoring at Treeline, Churchill, Manitoba, Canada. *Remote Sensing*, 4: 2133–2155.

Raudkivi, A. J., 1979: *Hydrology: An Advanced Introduction to Hydrological Processes and Modeling*. Pergamon, 479 pp.

Rott, H., Cline, D., Duguay, C., Essery, R., Haas, C., Macelloni, G., Malnes, E., Pulliainen, J., Rebhan, H., and Yueh, S., 2008: CoReH2O—a Ku- and X-band SAR mission for detailed studies of snow and ice monitoring. *In* Proceedings, European Conference on Synthetic Aperture Radar (EUSAR), 7th, 2–5 June. Friedrichshafen, Germany: VDA, 1–4.

Shi, J., and Dozier, J., 2000: Estimation of snow water equivalence using SIR-C/X-SAR, Part II: inferring snow depth and particle size. *IEEE Transactions on Geoscience and Remote Sensing*, 38: 2475–2488.

Sun, S., Che, T., Wang, S., and Wang, Z., 2013: Snow cover area retrieval using C-band SAR in mountain areas. *Remote Sensing Technology Application*, 28: 444–452.

Tsang, L., and Kong, J. A., 1981: Scattering of electromagnetic waves from random media with strong permittivity fluctuations. *Radio Science*, 16: 303–320.

Tsang, L., Kong, J. A., and Shin, R. T., 1985: *Theory of Microwave Remote Sensing*. New York: Wiley.

Tsang, L., Kong, J. A., and Ding, K-H., 2004: *Scattering of Electromagnetic Waves, Theories and Applications*. New York: Wiley.

Ulaby, F. T., and Stiles, W. H., 1980: The active and passive microwave response to snow parameters: 2. Water equivalent of dry snow. *Journal of Geophysical Research*, 85(C2): 1045–1049.

Ulaby, F. T., Moore, R. K., and Fung, A. K., 1981: *Microwave Remote Sensing: Active and Passive, Vol. I: Microwave Remote Sensing Fundamentals and Radiometry*. Boston: Artech House.

Ulaby, F. T., Moore, R. K., and Fung, A. K., 1982: *Microwave Remote Sensing: Active and Passive, Vol. II: Radar Remote Sensing and Surface Scattering and Emission Theory*. Boston: Artech House.

Ulaby, F. T., Moore, R. K., and Fung, A. K., 1986: *Microwave Remote Sensing: Active and Passive, Vol. III: Volume Scattering and Emission Theory, Advanced Systems and Applications*. Boston: Artech House.

Wang, J., Che, T., Zhang, L., Jin, R., Wang, W., Li, X., Liang, J., Hao, X., Li, H., Wu, Y., and Hu, Z., 2009: The cold regions hydrological remote sensing and ground-based synchronous observation experiment in the upper reaches of Heihe River. *Journal of Glaciology and Geocryology*, 31: 189–197.

West, R. D., 2000: Potential applications of 1–5GHz radar backscatter measurements of seasonal land snow cover. *Ratio Science*, 35: 967–981.

MS accepted October 2014

Downloaded From: https://complete.bioone.org/journals/Arctic,-Antarctic,-and-Alpine-Research on 16 Mar 2025
Terms of Use: https://complete.bioone.org/terms-of-use